applied sciences

MDPI

Article

Geophysical Study of a Large Landslide Affecting the Urban Area of Albuñuelas (S Spain)

Mara Mita [1], Juan José Galiana-Merino [2,3,*], Jesús Garrido [4], Luca Lenti [5], Salvatore Martino [6], Jacopo Pappadopoulo [7], José A. Peláez [8], Boualem Youcef Nassim Benabdeloued [3,9] and José Delgado [9]

1 Department of Géotechnique, Environment, Risques Naturels et Sciences de la Terre, Université Gustave Eiffel, 44344 CEDEX Bouguenais, France; mara-mita@univ-eiffel.fr
2 University Institute of Physics Applied to Sciences and Technologies, University of Alicante, Crta. San Vicente del Raspeig, s/n, 03080 Alicante, Spain
3 Department of Physics, Systems Engineering and Signal Theory, University of Alicante, Ctra. San Vicente del Raspeig, s/n, 03080 Alicante, Spain; nassim@ua.es
4 Department Civil Engineering, University of Granada, 18071 Granada, Spain; jega@ugr.es
5 Institut Français des Sciences et Technologies des Transports, de l'Aménagement et des Réseaux (IFSTTAR), Université Gustave Eiffel, 14-20 Boulevard Newton, Champs-sur-Marne, 77447 Marne la Vallée, France; luca.lenti@ifsttar.fr
6 Department of Earth Science and Research Centre for Geological Risk (CERI), Università di Roma "La Sapienza", 00185 Roma, Italy; salvatore.martino@uniroma1.it
7 Geo2Siena, 53100 Siena, Italy; pappadopoulo@geo2siena.it
8 Department of Physics, University of Jaén, 23071 Jaén, Spain; japelaez@ujaen.es
9 Department of Earth and Environmental Sciences, University of Alicante, Ctra. San Vicente del Raspeig, s/n, 03080 Alicante, Spain; jose.delgado@ua.es
* Correspondence: jj.galiana@ua.es

Abstract: The urban area of Albuñuelas, a small town located to the south of Granada (S Spain), has been developed in terrain affected by a large-scale rotational landslide with very slow rate of movement. Despite this situation, the internal structure of the landslide and how it has evolved to its present state has not been analyzed in depth up to now. In this paper, we present the first study performed on this landslide to define its configuration and characteristics. For this purpose, ambient noise single-station and array measurements were carried out along several cross-sections of the landslide. The inversion of the measurements has allowed for the estimation of the soil stratigraphy at each site of measurement. These geophysical results have been constrained by data from a borehole drilled in the zone and from field observations of the local geology, allowing for the reduction in uncertainties in the results. A geological–geophysical model of the landslide has been built from these data, showing that the landslide thicknesses is greater than 50 m in its central parts and above 60 m in the upper ones. This model reveals that the evolution of the landslide was complex, with several dislodged elements (blocks) that moved in sequence (retrogression) and were partially eroded in order to explain present morphology. The future evolution of this landslide will be controlled by the composition of the materials surveyed along the foot of the valley, being the western part where there are more erodible materials according to the obtained results.

Keywords: landslide; geological structure; geophysical prospecting; ambient noise; HVSR; array techniques

Citation: Mita, M.; Galiana-Merino, J.J.; Garrido, J.; Lenti, L.; Martino, S.; Pappadopoulo, J.; Peláez, J.A.; Benabdeloued, B.Y.N.; Delgado, J. Geophysical Study of a Large Landslide Affecting the Urban Area of Albuñuelas (S Spain). *Appl. Sci.* **2023**, *13*, 12205. https://doi.org/10.3390/app132212205

Academic Editors: Jangwon Suh and Sung-Min Kim

Received: 3 October 2023
Revised: 1 November 2023
Accepted: 7 November 2023
Published: 10 November 2023

1. Introduction

Managing landslide hazards requires the knowledge of both the hosting slope and the unstable mass. In general, the morphology and location of failure surfaces are fundamental for evaluating how the stability of a given landslide may evolve due to changes of different triggering factors [1,2]. These data are usually collected by drilling expensive boreholes. Although this procedure is very effective and allows for the retrieval of undisturbed samples that may be tested in laboratory to estimate geotechnical properties of the materials affected

by instability, it may become prohibitive when landslide mass is very large because the number of boreholes needed is too high. For these cases, geophysical methods represent an interesting solution because they allow for the fast coverage of wide areas at a reasonable cost, and they do not disturb the area under study [3–5]; this last characteristic is of special interest when the landslide affects urban areas. At present, electromagnetic [6,7], electrical [8,9] and seismic methods [10–12] are among the most used geophysical techniques applied to landslide studies.

The usefulness of these techniques is based in the consideration that there exists a contrast in the physical properties of the different materials involved (landslide mass versus stable slope). Limitations occur when such a contrast is due to presence of boundaries without interest in the slope stability problem. For instance, results of electrical methods are highly dependent of the presence of water in the medium, but it may not necessarily be related to the location of landslide boundaries [5]. Another drawback may also be associated with the characteristics of the terrain under study. For example, the particular case of our study, the Albuñuelas landslide, is characterized by an irregular relief, with difficulties in access and the availability of space. In these conditions, the application of some geophysical techniques, such as electrical techniques, would be quite complicated due to the extension of wiring that would be required to be able to investigate the expected depths.

In the case of seismic methods, those based in the analysis of ambient noise (passive methods) have gained popularity in recent times [5,13–15]. The basis of these techniques is to find the contrast of mechanical properties between a deep and rigid basement, and a layer (or multiple layers) of softer material resting on this basement. The study may be performed through single stations equipped with triaxial sensors (HVSR technique) [16] or by arrays of vertical sensors analyzed using the spatial autocorrelation (SPAC) method [17], the extended spatial autocorrelation (ESAC) analysis [18,19] or the frequency-wavenumber (*f-k*) transform [20,21], among other possible methods. The HVSR method provides the fundamental resonance frequency of SH waves (e.g., [22]), while surface waves dispersion curves result from array data (e.g., [19,23,24]). Both type of results can be inverted, providing a soil column depicting the local stratigraphy, where each layer is characterized by its thickness and shear wave velocity [25,26].

The town of Albuñuelas (Granada province) is located close to the southern border of the Granada basin (Figure 1) and was built on a slide (Figure 2), which is characterized by a very low rate of movement [27]. This town was destroyed during the Andalusia earthquake (24/12/1884), Mw 6.5 [28] (Figure 1), with the oldest houses in the town being those rebuilt after the earthquake. Currently, these older houses are rotated at angles of up to 6 degrees (Figure 2). This was initially interpreted as due to the accumulated landslide displacement after the reconstruction of the town [27]. However, data from the systematic measurement of the tilting of houses [29] and from SAR interferometry [30] seem to point out that a complex pattern of progressive ground settlement may also explain the observed tilting. Despite the menace that landslide movement may represent to this town, the geometry and structure of landslides remain unknown. This represent a serious drawback for conducting studies for the evaluation of the hazard, i.e., that a given increase in the rate of movement may be present in this town.

In this work we present the design, development and results of a geophysical study carried out in this landslide site. For this purpose, we have used several geophysical techniques based in the measurement of ambient noise and the results have been constrained by field (structural and geomorphological) data, as well as with data coming from a borehole specifically drilled for this study. The aim of this study is to apply well-known passive seismic methods to estimate the extent of the landslide and the depth to the failure surface, providing a complete model of its structure. This knowledge will contribute to understanding the behavior of this landslide and allow for future studies to be carried out about its behavior due to different triggering factors (scenarios of intense rain periods, river undercut or severe seismic shaking).

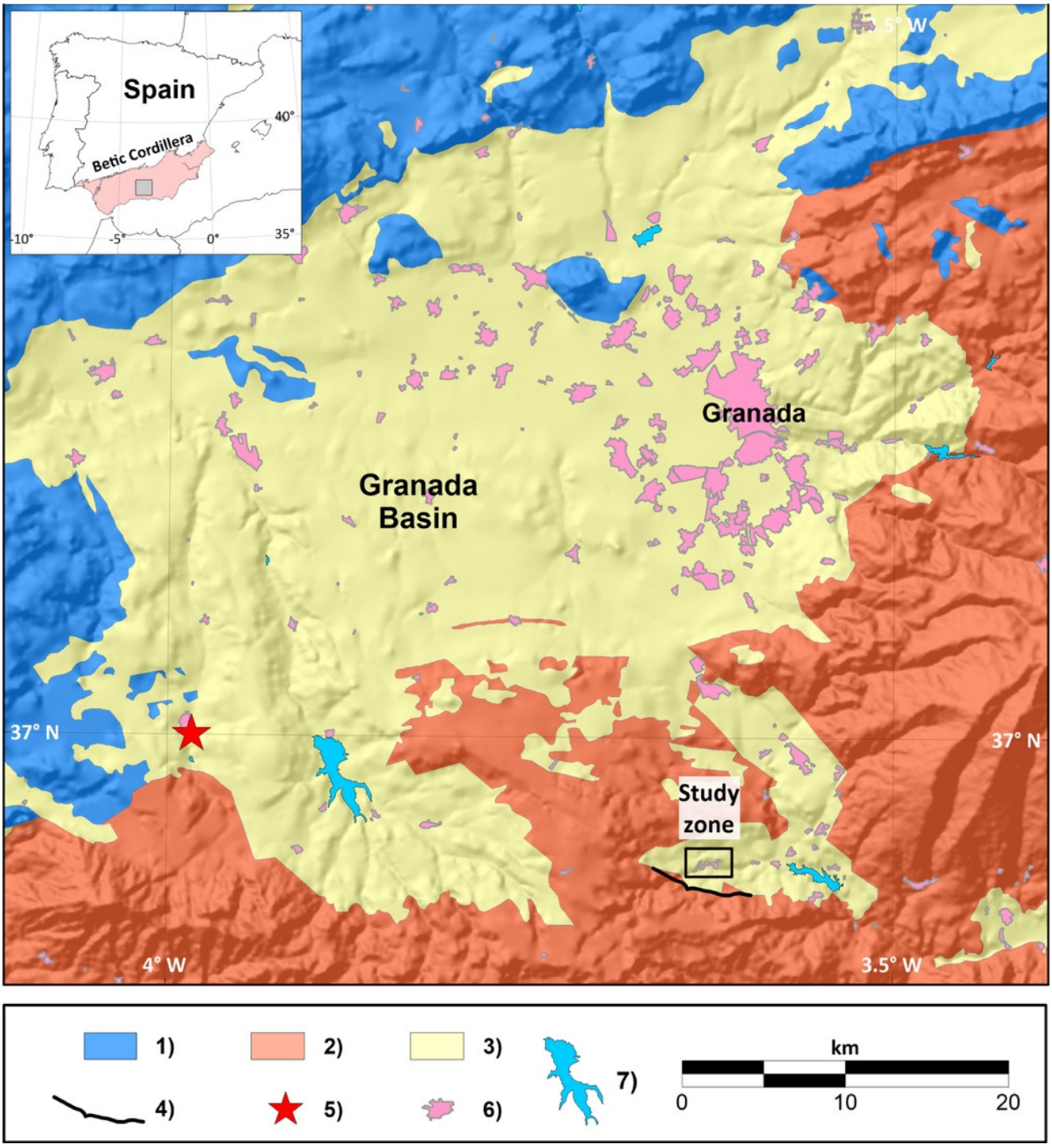

Figure 1. Location map of the study zone. (1) External Zones of the Betic Cordillera; (2) Internal Zones of Betic Cordillera: (3) Neogene–Quaternary rocks and sediments; (4) trace of the Albuñuelas fault [31]; (5) approximate location of the 1884, Mw 6.5, earthquake; (6) urban areas; (7) dams.

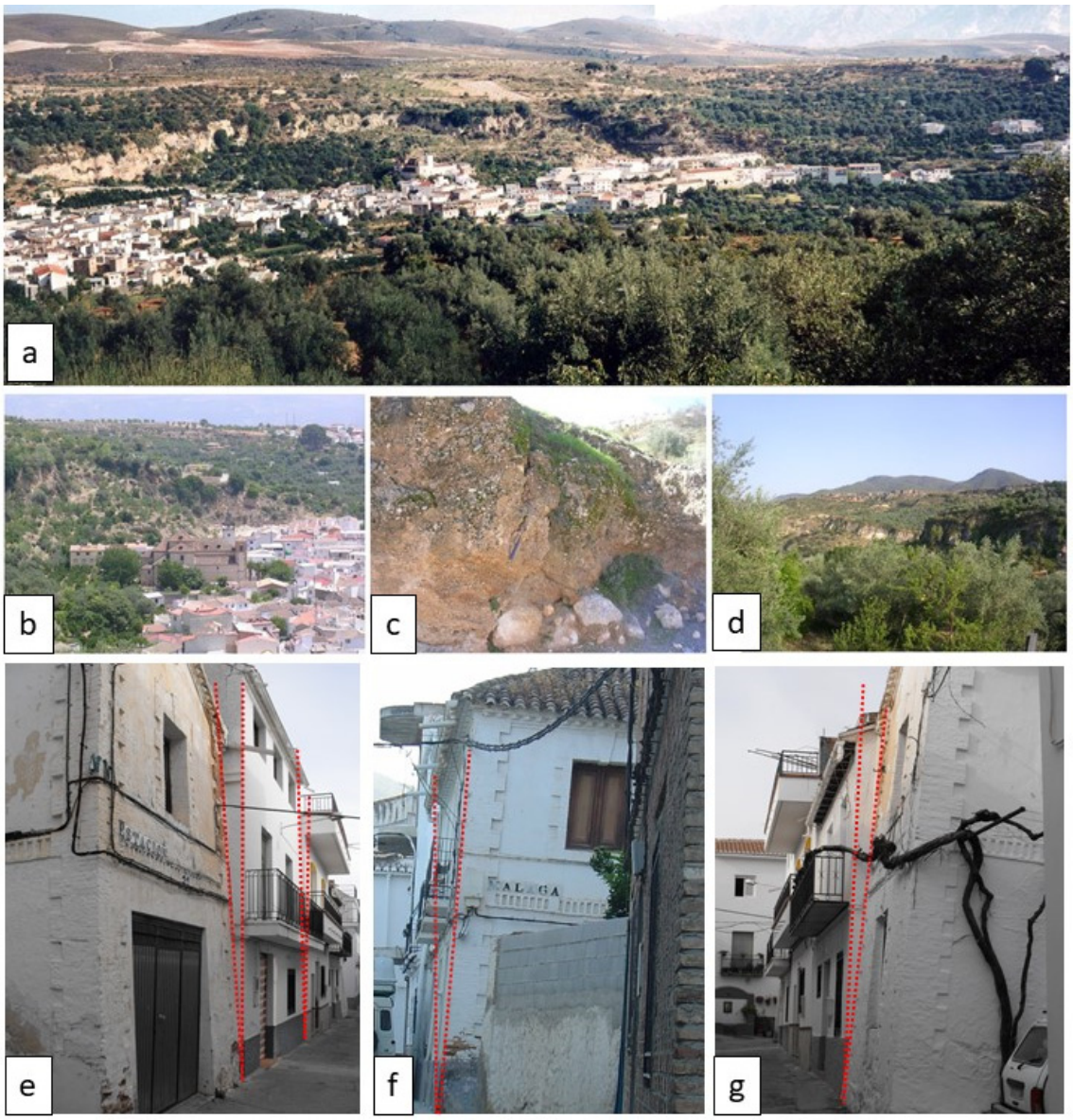

Figure 2. (**a**) General view of Albuñuelas. It is noticeable that the escarpment is almost 50 m high and composed of calcarenite behind the town. (**b**) Zoomed view of the main scarp of the Albuñuelas landslide close to the main church. (**c**) Back-tilted conglomerates inside the Albuñuelas landslide mass. (**d**) Landslides affecting the slope in front of the town of Albuñuelas (south slope of the Albuñuelas valley) revealing a diffused rotational mechanism. (**e**–**g**) Examples of tilted houses.

2. Geological Setting

The study zone is located in the Granada Basin (Figure 1). This is a Neogene intramountain basin in the boundary between the External and the Internal Zones of the Betic Cordillera. It is located in the central part of the cordillera, where seismicity is frequent and some destructive earthquakes have struck the area [28,32,33].

The basement of the Granada Basin is constituted by Mesozoic sedimentary rocks from the External Zones of the Cordillera to the north and west borders of the basin, and by Palaeozoic to Triassic metamorphic rocks from the Internal Zones in the south and east borders (Figure 1). The basin fill comprises sedimentary rocks from Burdigalian (Miocene) up to Quaternary [34,35]. In the study zone, the basement is formed by marbles and schists of the Alpujárride Complex (Internal Zones of the Cordillera). They outcrop to the south of the study zone, limited by the Albuñuelas fault (Figure 1). According to [36], a very small

outcrop of these materials exists in the lower part of the valley, south of the town, in the vicinity of the Saleres River. Unfortunately, this outcrop could not be identified in the field work conducted for this study because the area was covered by recent sediments provided by the river.

The stratigraphic record of the basin starts with continental red silts that have a thin layer of grayish blue clays on top, Serravallian in age, and are in direct contact with the basement. Above them, reef sandstone and calcarenite with abundant marine fauna (lower Tortonian) and red-orange conglomerates and silt, a poorly cemented and deposited in a marine environment (Upper Tortonian in age), are found. Finally, on top of all these materials, there are continental conglomerates, associated with the glacis that formed in the area during the Pliocene and Quaternary, in recent hillside deposits along slopes and alluvial sediments in the lower part of the valleys, deposited by the rivers that run through them.

From measurements made in outcrops, red silts are about 60 m thick, reef sandstone and calcarenite have a highly variable average thickness, but it seems that they do not exceed 55 m as a whole (10 m for reef sandstones and 45 m for calcarenites), and red–orange conglomerates and silts have very variable thickness, with a maxima estimated at several hundreds of meters [37,38]. The remaining units (recent materials) have very variable thickness, depending on size of outcrop and position on the slopes. This sedimentary sequence is folded and faulted [38,39]. They show a general dip towards the south, where the so-called Albuñuelas fault constitutes the southern limit of the basin (Figure 1).

Shear strength data of materials in this zone are scarce. D'Angiò [40] presented results obtained from undisturbed block samples of red silts unit, tested in triaxial shear box tests, resulting an average friction angle of 33° (±2°) and a cohesion of 40 kPa. Román-Herrera et al. [41] compiled data of shear strength for marbles and schists in areas close to the study zone. According to these authors, average values of friction angle and cohesion are 36° and 13.7 kPa, respectively, but these values increase to >40° and >200 kPa when marbles are present. No data are available for other formations in the study zone.

Landslides are common in the Granada Basin [42]. El-Hamdouni [43] studied this problem in the southeast border of this basin and inventoried several hundreds of landslides. The neighborhoods of the town of Albuñuelas have grown by occupying terrains affected by several of them (Figure 3). The main neighborhood has been developed on a rotational slide (sensu [1]; Figure 2). It is 850 m wide and 600 m long (approx.) and has its body broken into several parts (or blocks), each with different amount of movement and rotation, limited by scarps that can reach tens of meters in some cases (Figure 2). In the upper part of the landslide, some of these blocks contain minor slides affecting small volumes of red–orange conglomerates, showing notable rotation (30–40° towards the inner part of slope; Figure 3). Because of their small size, these minor slides were not mapped and presented in Figure 3. Overall, the movement of landslides occur from NW towards SE.

To the east of the town, another neighborhood of the town has been developed on a complex landslide (Figure 3), showing slide movement in the upper areas of the body, and becoming a flow towards the landslide toe. It is 250 m wide and 900 m long (approx.), with movements in a N-S direction. Between these two landslides, and limited by their flanks, another smaller one exists (Figure 3). In all cases, landslides affect the Miocene sequence of materials.

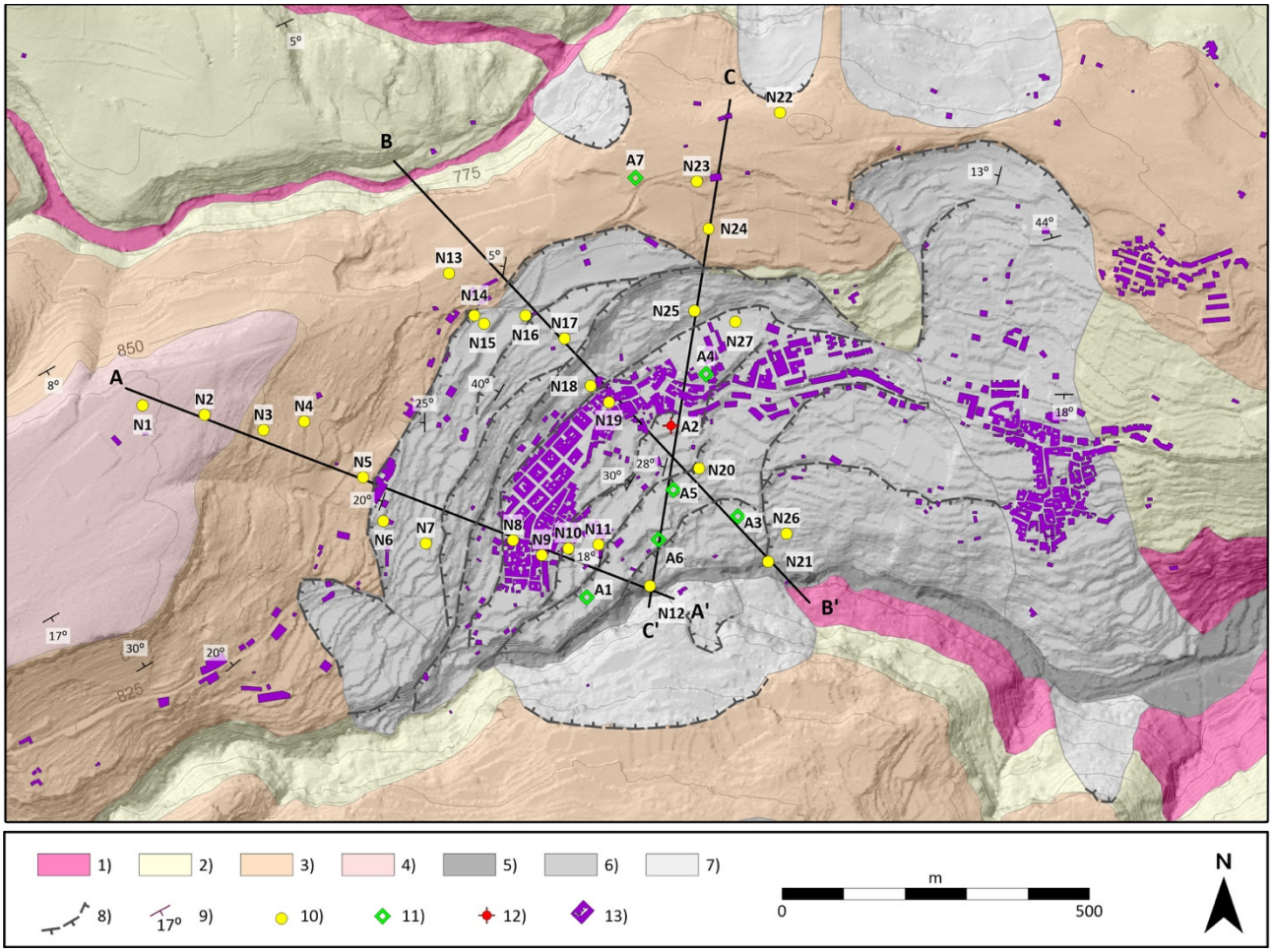

Figure 3. Geological map of the Albuñuelas area showing the location of the measurement sites. (1) Red silts (Serravallian); (2) reef sandstone and calcarenite (Lower Tortonian); (3) red–orange conglomerates and silt (Upper Tortonian); (4) conglomerates (Pliocene–Quaternary); (5) alluvial sediments (Quaternary); (6) slope debris (Quaternary); (7) landslide (Quaternary); (8) landslide scarp; (9) strike and dip of beds; (10) single station measurements (HVSR); (11) array measurements; (12) borehole drilled + HVSR + Array; (13) blocks of houses.

3. Geophysical Methods

3.1. H/V Method

The HVSR or H/V technique is broadly employed for the rapid detection and assessment of seismic amplification effects by measuring ambient vibrations (or seismic noise) with just a single three-component station. This technique requires the acquisition of three components of the ground motion and consists of obtaining the ratio between the horizontal and vertical Fourier spectrum. This ratio, which is expressed as a function of the frequency, is called the H/V (or HVSR) curve (or function). The frequency peaks (or H/V peaks) found in this spectral ratio provide a direct estimation of the seismic resonant effects of the soil under study (e.g., [15,44–51]). The resonant frequencies reflect impedance contrasts found between sedimentary layers and especially between the sedimentary cover and the bedrock.

This method was first introduced by [52], and then revised by [16]. These authors highlighted the correlation between the frequency value of the H/V peak and the fundamental resonance frequency of the site (f_0), suggesting the ability of this technique to provide information on the dynamic characteristics of the subsoil. From these considerations, the well-known Equation (1) is derived [44],

$$f_0 = \frac{V_S}{4 \cdot h} \quad (1)$$

relating the resonant frequency (f_0) with the average shear-wave velocity (V_S) and the thickness (h) of the sedimentary layer.

According to [53], the H/V analysis can be used for estimating the possible seismic impedance contrasts, taking into account the frequency peaks; defining the lithological and geological formations constituting the sedimentary cover and the bedrock; and creating a map of the resonance frequency along an urban area, which defines the limits of the more dangerous areas in terms of soil-building structure resonance.

3.2. f-k Analysis

The method based on the frequency-wavenumber (*f-k*) analysis [20,21] is applied on seismic array measurements for estimating the propagation velocity of the Rayleigh waves as a function of the frequency (i.e., dispersion curve).

The *f-k* analysis estimates the power spectral density function of the recorded seismic noise in the frequency-wavenumber domain. This function describes the phase and amplitude of the plane waves propagating in the *x*-*y* plane of the array with velocities and directions defined by the two-dimensional horizontal wavenumber vector $|\vec{k}|, (k_x, k_y)$. Specifically, considering the pulsation of the plane waves, $\omega = 2\pi f$, the wavenumber vector $|\vec{k}|$, is related to the phase velocity $\vec{v}$ and the propagation angle β of the signal by Equation (2):

$$\begin{aligned} \left|\vec{v}\right| &= \frac{\omega}{|\vec{k}|} = \frac{\omega}{\sqrt{k_x^2 + k_y^2}} \\ k_x &= \frac{\omega}{v_x} = \frac{\omega \cdot cos(\beta)}{\left|\vec{v}\right|} \\ k_y &= \frac{\omega}{v_y} = \frac{\omega \cdot sin(\beta)}{\left|\vec{v}\right|} \\ \beta &= arctan\left(\frac{k_y}{k_x}\right) \end{aligned} \quad (2)$$

For each of the analyzed frequencies, $\omega = 2\pi f$, and the absolute maximum of the power spectral density in the (k_x, k_y) plane is identified, which directly provides the phase β and the propagation velocity $\left|\vec{v}\right|$ of the incoming plane waves.

There are two different approaches to obtain the power spectral density in the (k_x, k_y) plane: the maximum likelihood method (MLM) [20] and the beam-forming method (BFM) [21]. The last method is the one used in this study.

3.3. Inversion of the Dispersion and H/V Curves

The H/V and/or dispersion curves can be inverted to obtain an estimation of the shear-wave velocity profile in the site under study. These curves present different sensitivities with respect to the characteristics of the sedimentary cover. While the dispersion curve can provide more detailed information on the different sediment layers, the H/V curve can more reliably determine the total thickness of the sedimentary cover from the resonant frequency, reflecting the contrast between sediments and basement rocks. Thus, a joint-inversion of H/V and the dispersion curve (e.g., [25,54,55]) would be preferred, as long as possible, to obtain more detailed V_S profiles of the subsoil.

The inversion of the experimental data has been conducted following the neighborhood algorithm [56,57], which is a stochastic direct research method for non-linear inversion. The inversion process explores a huge number of possible solutions or models with a certain number of sedimentary layers, whose properties (S-wave velocity, P-wave velocity, density and layer thickness) are within preset margins. In general, prior knowledge of the type of soil through some geotechnical method (e.g., borehole drills and downhole experiments) helps to restrict the number of layers and their corresponding thickness, as well as the S-wave velocity ranges. Density and Poisson's ratio have been established for

all layers in the range of 1600–2200 kg/m^3 and 0.2–0.5, respectively, which corresponds to the characteristics of the materials in the studied landslide.

The theoretical response of each of the models obtained as a solution (in terms of ellipticity of the fundamental mode Rayleigh wave or the dispersion curve) is contrasted with the corresponding experimental curves by means of a misfit function [58], given as the result of how much the provided solution fits the type of soil under study.

4. Data Acquisition and Analysis

4.1. Borehole

There are no boreholes available within the landslide body that could help in constraining the interpretation of geophysical data for this study. There was a borehole drilled by researchers of the University of Granada, but log-stratigraphy was not available. To avoid this lack of data, a single borehole was specifically drilled for this study by a geotechnical laboratory (Centro de Geotecnia y Control de Obras S.L., company). The borehole reached 48 m of depth and was stopped due to limitations in available funds.

Figure 4c shows the soil column found in the borehole. The following can be observed: (a) a shallow, 1.0 m thick layer of man-made debris; (b) a 9.6 m layer of brown to red clayey silt and conglomerates; (c) at 10. 6 m deep, yellow, poorly cemented sandstone and clayey sand; and (d) below these materials, the soil column is composed by gray clay (3.5 m) and red silt (28 m), including levels of sandstone and conglomerates. These conglomerates become more frequent towards the end of the borehole. Unfortunately, the borehole stopped before reaching the base of red silts and the basement. During drilling works, an aquifer in relation with sandstones was recognized, with the rest of the soil column in the borehole remaining dry.

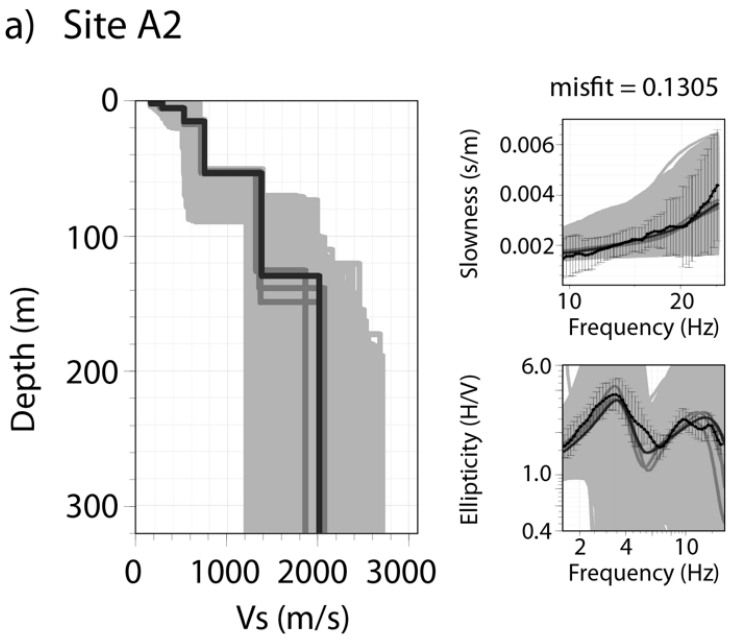

Figure 4. *Cont.*

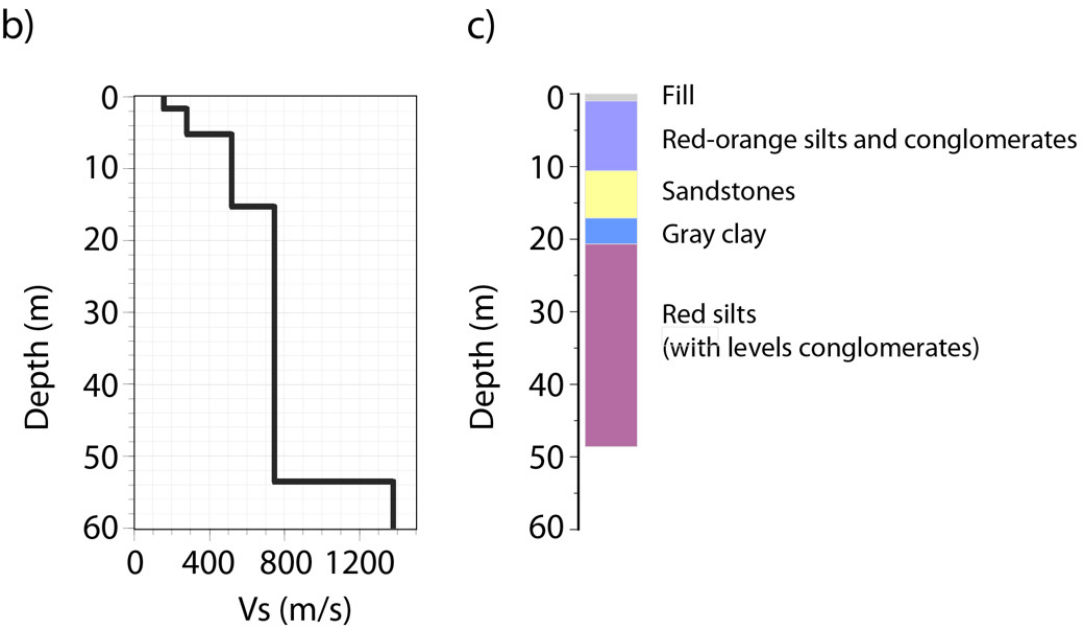

Figure 4. (**a**) S-wave profile obtained by joint-inversion of H/V and dispersion curves at the borehole site (site A2). On left panel, the minimum misfit model (black) is shown together with the models comprising inside the minimum misfit + 10% (dark gray) and all the tested models (light gray). On the right panels, the mean value plus standard deviation bars of the experimental H/V curve (right bottom panel) and dispersion curve (right top panel) are shown in black together with the ellipticity/slowness curves associated with the best-fitting model (darkest gray), minimum misfit + 10% (dark gray) and all the other tested models (light gray). The minimum misfit value is shown above the right panels. (**b**) Comparison of the first 60 m of the best-fitting model with, (**c**) the stratigraphic column obtained from the borehole drill.

4.2. H/V Measurements

With the aim of retrieving the information about the stratigraphy of the landslide and nearby areas, ambient noise measurements were taken in 26 different sites in the study area. The location of these sites was selected in order to obtain information along cross-sections of the main landslide where the town was built and considering the distribution of diverse bodies constituting the landslide (Figure 3). In any case, it was not always possible to measure at the planned sites due to access limitations (no permissions were given, in some cases, by the property owners for performing the measurements). Distance between sites varies from several dozens to about 100 m in the more distant sites (Figure 3). When field work was designed, an attempt was made to ensure that the distance between points did not exceed 50 m, but when all the planned sites were established, access to some places were not possible, so these initial estimations had to vary to the final positions shown in Figure 3. Other measurements were taken along the upper parts of the slope, outside of the landslide, to obtain information about the distribution (thickness) of materials in stable areas.

The measurements were performed through Guralp CMG-6TD broadband stations. The recording duration was approximately 60 min, which was enough to ensure the statistical stabilization of the signal. The sampling frequency was set to 100 Hz, and the data saved in Guralp Compress Format (GCF). Geopsy software (www.geopsy.com) were used for the H/V analysis of data. First, the data were baseline corrected; then, the signals were each divided into windows of 40 s length and analyzed separately. The time windows were tapered using a Hanning function to avoid the leakage phenomena, and the corresponding spectra were smoothed using a triangular moving window with frequency dependent half-width (5% of central frequency).

The reliability of the obtained H/V curves has been checked through the guidelines established in the SESAME project [59].

4.3. f-k Experiment

Seismic noise array measurements have been analyzed through the *f-k* technique, providing an estimation of the Rayleigh wave-phase velocity dispersion curve.

In the present study, 2D arrays were deployed at seven different sites along the landslide. The equipment used consisted of twelve 4.5 Hz vertical geophones connected to a multichannel seismic recorder (SmartSeis ST), which allows for the retrieval of dispersion curves above approximately 2 Hz [60,61]. The geophones were deployed following a circular or rectangular layout with a maximum aperture of 16–20 m, depending on the available space. Considering that the wavelengths estimated by the *f-k* method can be several times greater than the maximum aperture [55,62], these configurations would be sufficient for soil classification purposes [63]. The recording duration was 30–45 min with a sampling frequency of 500 Hz, although it was subsequently resampled at 100 Hz.

The data analysis was performed using Geopsy software (www.geopsy.com). The raw signals were previously processed in the same way as indicated for the H/V analysis (Section 4.2).

5. Results

5.1. Geophysical Results at the Borehole Site

In this study, the information provided by the borehole drill has been used as starting point for the estimation of the *Vs* profile at the center of the landslide. According to the stratigraphy of the place, three main different layers of materials can be considered: silt and conglomerates, sandstone and red silt. In addition, a surface layer of alteration and/or accumulated fills are also observed.

At the borehole site, H/V and array measurements were taken in order to combine the analysis of the seismic passive techniques with the geotechnical information and assess the reliability of the obtained results. According to that, the joint-inversion of the H/V and dispersion curves has been accomplished considering the number of layers and the ranges of thickness deduced by the stratigraphic information obtained from the borehole drill.

The Dinver software of the Sesarray package (www.geopsy.org) has been used for carrying out the joint-inversion and estimating the corresponding *Vs* profile at the borehole site.

In Figure 4a, the *Vs* profile estimated from the joint-inversion of H/V and array measurements at the borehole site is presented. The model with the minimum misfit (black), the models below the minimum misfit + 10% (dark gray) as well as all the tested models (light gray) are shown in the left column. The ellipticity and the dispersion curves corresponding to the best estimate model (darkest gray), the models below the minimum misfit + 10% (dark gray) and all the analyzed models (light gray), are shown together with the experimental curves (black) on the right side.

In Figure 4b,c, the stratigraphic information obtained from the borehole drill is compared to the best *Vs* profile (i.e., the model with the minimum misfit) estimated at the first 60 m.

As a result, a shallow layer of fills is estimated with an S-wave velocity of 160 m/s and an approximately thickness of 2 m. Below, a first layer, associated with the silt and conglomerate materials, is characterized by a *Vs* of 280 m/s and thickness of 4 m. The second estimated layer reaches a depth of 15 m, with a S-wave velocity of 520 m/s. This layer is associated with the sandstone materials. Finally, the third layer presents a *Vs* of 750 m/s and reaches a maximum depth of 52 m, corresponding with the red silt materials.

The obtained results show that the model with the minimum misfit correctly identifies the different layers. The velocity values estimated for each layer are in agreement with the properties of the materials observed in the stratigraphy column. In the case of the thicknesses, it is observed that a slight underestimation of 3–5 m in the most superficial layers, which falls within the margin of the minimum misfit + 10% observed in Figure 4a.

5.2. S-Wave Velocity Profiles

Once this first *Vs* profile is obtained, situated purposely in the central part of the landslide, the analysis of the other sites was performed going from the nearest points to the furthest ones, situated on the top of the hill and the proximity of the Saleres River. In this way, the connection between the adjacent sites has been taken into consideration, obtaining coherent *Vs* profile results along the studied landslide.

Dinver software from the Sesarray package (www.geopsy.org) was used to carry out the single- or joint-inversion and to estimate the corresponding *Vs* profile in all the selected sites. In some places, it was not possible to deploy an array, so only H/V measurements were used for the inversion process.

Figures 5 and 6 show some examples of *Vs* profiles estimated by single- or joint-inversion of the H/V and dispersion curves. The model with the minimum misfit (black), the models below the minimum misfit + 10% (dark gray) as well as all the tested models (light gray) are shown in the left column. The ellipticity and the dispersion curves corresponding to the best estimate model (darkest gray), the models below the minimum misfit + 10% (dark gray) and all the analyzed models (light gray), are shown together with the experimental curves (black) on the right side.

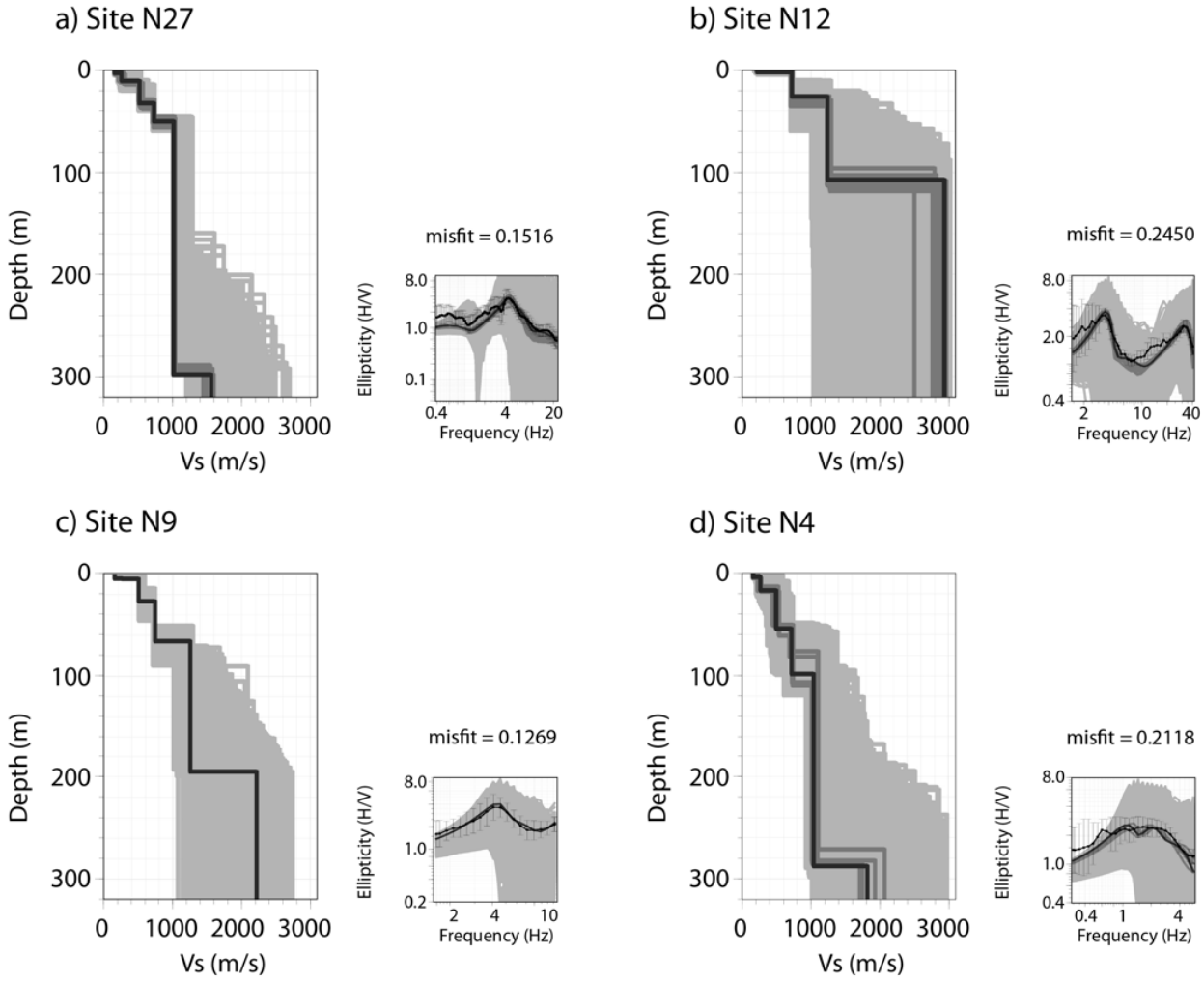

Figure 5. *Cont.*

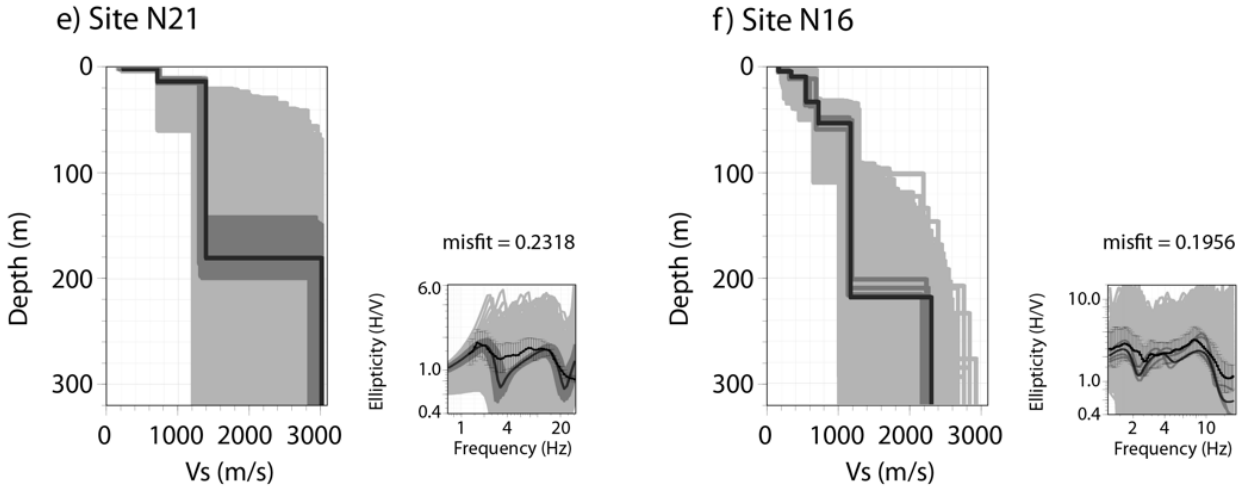

Figure 5. Examples of S-wave profiles obtained by inversion of H/V curves at six different sites of the landslide: (**a**,**b**) Sites N27 and N12 (east cross-section); (**c**,**d**) sites N9 and N4 (west cross-section); (**e**,**f**) sites N21 and N16 (central cross-section). On the left panel, the minimum misfit model (black) is shown together with the models comprising inside the minimum misfit + 10% (dark gray) and all the tested models (light gray). On the right panel, the experimental H/V curve (mean value plus standard deviation bars in black) is shown together with the ellipticity curve associated with the best-fitting model (darkest gray), minimum misfit + 10% (dark gray) and all the other tested models (light gray). The minimum misfit value is shown above the H/V plot.

All the analyzed H/V curves exhibit one or more evident peaks due to the resonance effect associated with the impedance contrast between the different layers or stratums. Thus, the principal interfaces have been clearly identified after the inversion process. Moreover, the presence of resonance peaks in the H/V curves also indicates possible amplification phenomena, which constitutes an important parameter for site response studies and for future seismic hazard studies in this area.

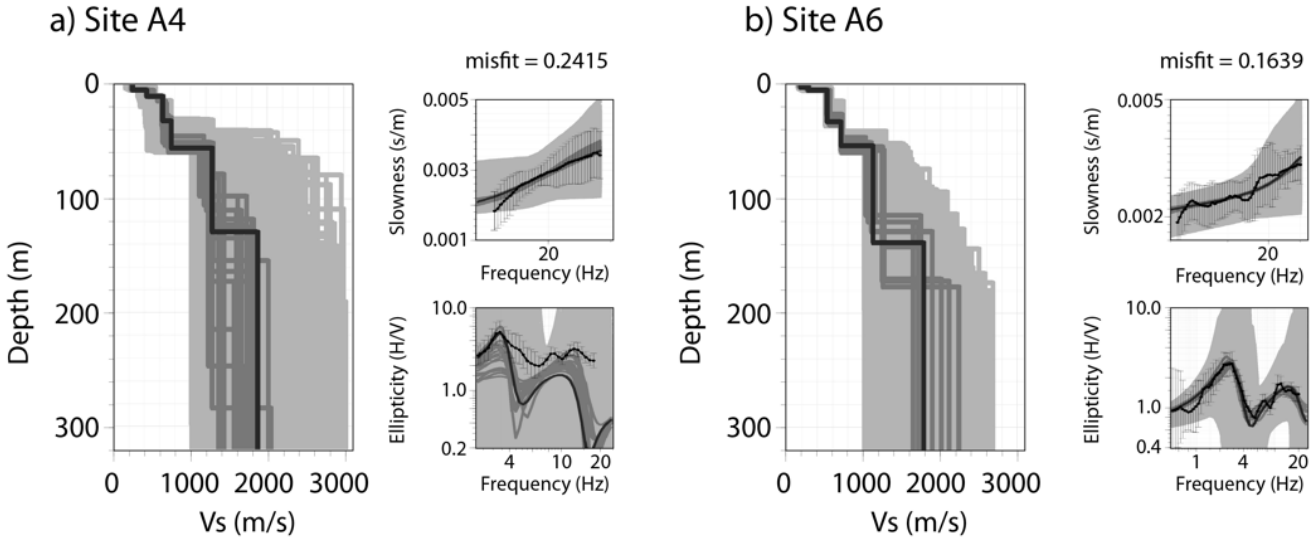

Figure 6. *Cont.*

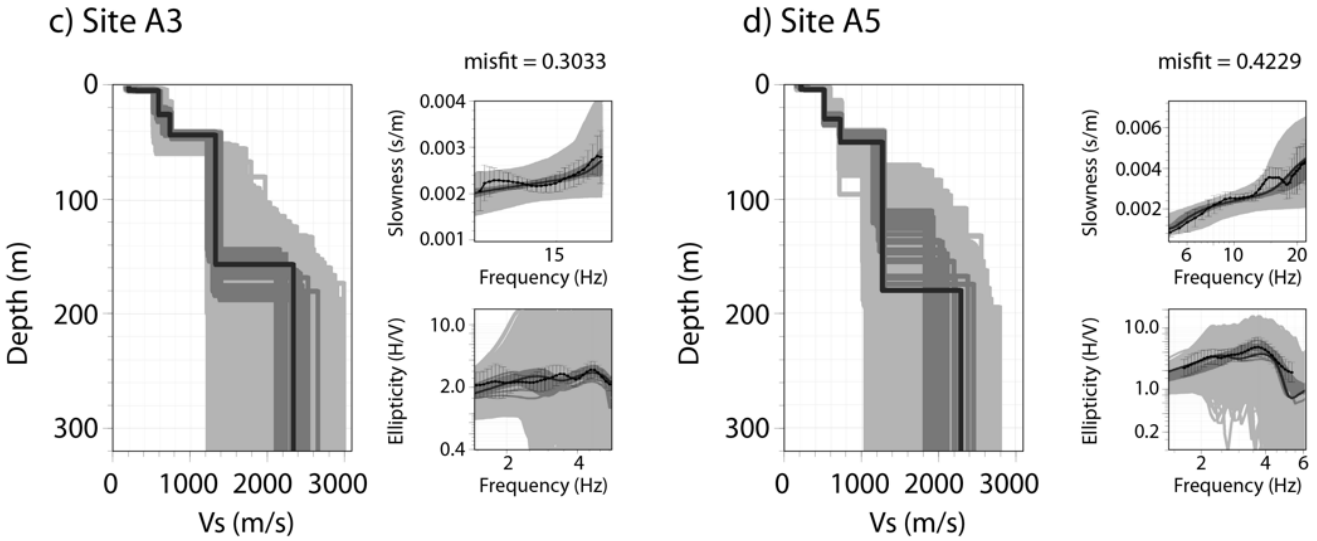

Figure 6. Examples of S-wave profiles obtained by joint-inversion of H/V and dispersion curves at four different sites of the landslide: (**a**,**b**,**d**) Sites A4, A6 and A5 (west cross-section); (**c**) site A3 (central cross-section). On the left panel, the minimum misfit model (black) is shown together with the models comprising inside the minimum misfit + 10% (dark gray) and all the tested models (light gray). On the right panels, the mean value plus standard deviation bars of the experimental H/V curve (right bottom panel) and dispersion curve (right top panel) are shown in black together with the ellipticity/slowness curves associated with the best-fitting model (darkest gray), minimum misfit + 10% (dark gray) and all the other tested models (light gray). The minimum misfit value is shown above the right panels.

In most of the obtained dispersion curves, it is observed that the Rayleigh wave-phase velocity decreases with the increasing frequency, which is typically associated with simple stratigraphic conditions where shear-wave velocity consistently increases with depth. In some sites, especially in the sites where conglomerates emerge, the observation of a kink or flat zone in the experimental dispersion curve could be indicative of the presence of a soft layer below a stiffer one [55], which is subsequently confirmed by the estimated *Vs* profiles.

5.3. Stable Areas

The first step in our study was verifying if the obtained results were congruent with the data gathered from outcrops of the same geological formations in this zone. For this purpose, we focused on the results obtained from sites not affected by landslides, for which a complete soil column is available. As it was previously mentioned in Section 2, observed outcrops presented a red silt unit approximately 60 m thick, together with reef sandstone and calcarenite units with highly variable thicknesses that do not exceed 55 m (10 m for reef sandstones and 45 m for calcarenites) [37,38]. The results obtained at these sites on stable areas are presented in Figure 7. In this figure, we consider that the lower layer corresponds to the basement (marbles and schists), and according to the stratigraphy of the area, the units above represent the red silt, reef sandstone and calcarenite, red-orange conglomerates and silt, and continental conglomerates (only at sites N1 and N2), respectively. Finally, a thin layer of very low velocity is observed on the surface, which may be attributed to altered materials or artificial fills.

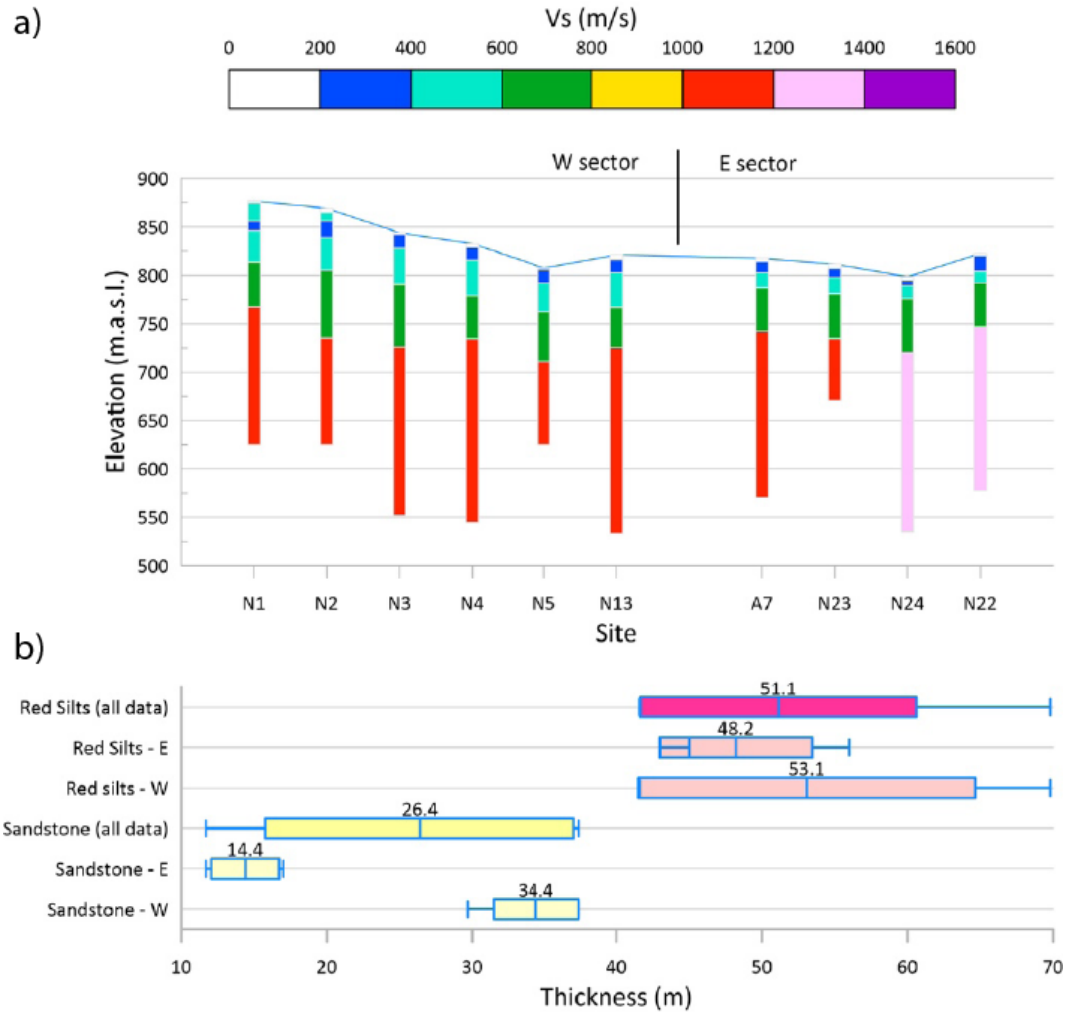

Figure 7. (**a**) *Vs* profiles obtained at sites located outside of landslide areas. (**b**) Distribution of *Vs* velocities for the red silt and sandstone units. Numbers show average thickness for each unit and zone. See Figure 3 for location of sites in this figure.

The obtained results show that *Vs* velocities in the basement are high, typically above 1000 m/s. Above the basement, the red silt layer is characterized by *Vs* velocities in the range of 600–800 m/s. The thicknesses of this unit show some variability, with values varying from 42 m (site N13) up to a maximum value of 70 m (site N2). Figure 7 shows that sites located in the eastern part of the study zone show lower thicknesses and dispersion, but values obtained are similar to those estimated in the western part of the study zone. It is noticeable that these values agree with data known from outcrops, showing differences lower than 10 m with respect to outcrop data (average value of 52 m vs. 60 m).

The results obtained for the reef sandstone and calcarenite unit (layer above red silt) (Figure 7) present *Vs* velocities in the range of 400–600 m/s and thicknesses with notable differences depending on the considered sector. For sites located in the western part of the study zone, the thicknesses vary in the range of 33–37 m (average value of 35.4 m). On the contrary, this same material shows lower thicknesses in the eastern sector of the study zone, between 12 and 17 m (14.4 m in average). These data seem to point out that this layer diminishes its thickness towards the east in the study zone. From the outcrop data, it is important to remark that this unit shows high variability in thickness, so the values obtained are consistent with the data obtained from this formation.

5.4. Landslide Geological Structure

The results obtained from the ambient noise measurements have been used in conjunction with the soil column information obtained from the borehole and the geological data (position of landslide scarps, material outcropping at ground surface, and dip and dip direction of beds in the landslide area) to model three cross-sections of the Albuñuelas landslide (Figures 8 and 9). The location of these three sections is shown in Figure 3.

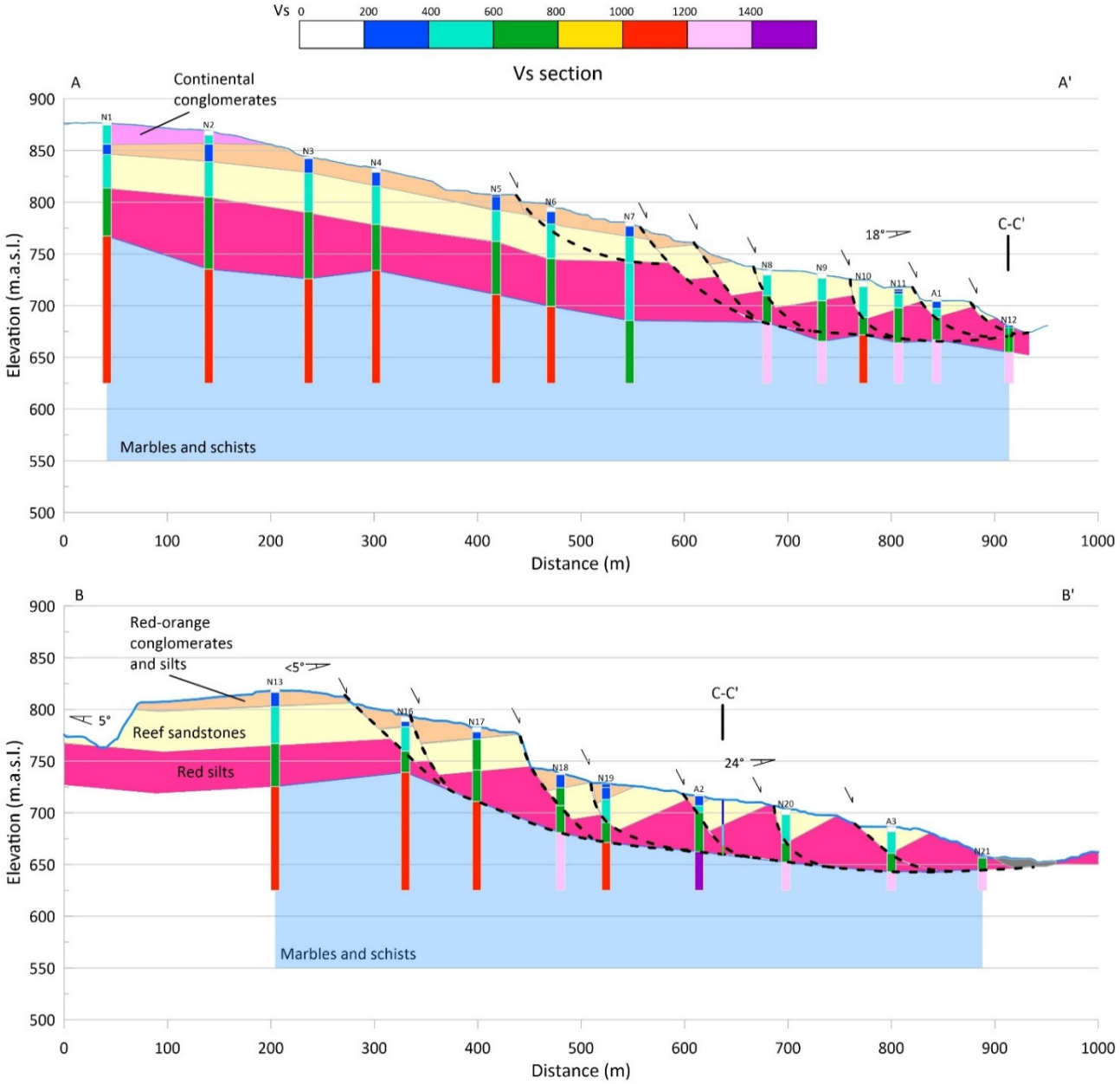

Figure 8. Longitudinal cross-sections of the Albuñuelas landslide showing the estimated position of the successive slides that constitute the landslide. Plot shows apparent dips used to build the model. Plot limits depth of the lowest layer to 625 m of elevation for clarity purposes. See Figure 3 for location of cross-sections. Arrows mark the position of scarps in landslide body.

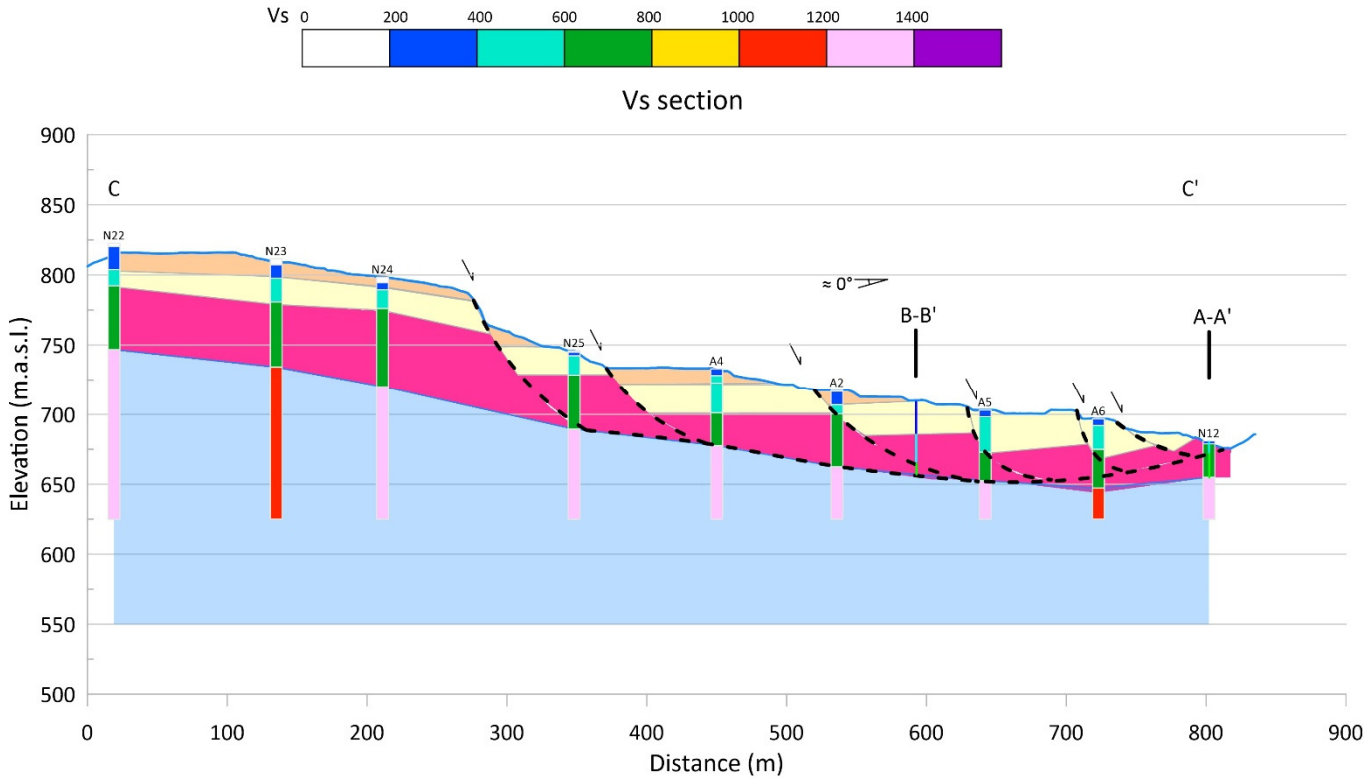

Figure 9. Transversal cross-section of the Albuñuelas landslide. Figure follows the same colors scale shown in Figure 8. See Figure 3 for location of cross-section. Arrows mark the position of scarps in landslide body.

The results obtained in the stable areas (see Section 5.3) have been useful for identifying the zones in each cross-section where thicknesses of red silt and/or sandstone (reef sandstones and calcarenites) agrees with the average values observed in stable zones, or where they show thicknesses lower than the expected ones. In this last case, it was interpreted as due to the presence of a failure surface, which cuts such a unit, reducing its thickness. For constructing these plots, we also considered the relative angle between each cross-section and the bed's dip-direction, to use a geometrically consistent dip in the plots. The apparent dip was computed by Equation (3):

$$tan\beta' = cos\alpha \cdot tan\beta \quad (3)$$

where α is the angle between the line of the cross-section and dip direction of beds (approx. N285° E to N300° E, depending of the site), β is the real dip of beds, and β' is the apparent dip of beds along the cross-section. Section A–A' (Figure 8) is approximately parallel to the dip direction of beds in the landslide area ($\alpha = 0°$), so units are presented with their real dip. Section B–B' forms an angle of approximately 30° with the dip direction of beds and units show a dip slightly lower than the measured one (24° vs. 28°). Finally, section C–C' is almost perpendicular to bed's dip direction ($\alpha \approx 90°$), so materials were arranged horizontally in this cross-section (Figure 9).

With the previous considerations, the obtained results show that upper limit of high velocity unit (basin basement) draws a surface dipping toward the south (right border of plots), where the Albuñuelas Fault is located, from approximately 750 m.a.s.l. in the northern part of sections to 650 m in the opposite side. Additionally, the sedimentary cover is thinner towards the southern part of sections, reaching the lowest values at the base of the valley where the basin basement should be found a few meters below ground surface in section B–B' (Figure 8, bottom). This agrees with the map prepared by [36], showing where it is very likely that recent sediments provided by the Saleres River buried the outcrop mapped by these authors. In the upper parts of the slope, sedimentary units also dip

toward the south with the exception of section B–B′, where a broad syncline exists in the top of the area (Figure 8).

6. Discussion

The proposed model obtained after the integration of all available data show a rotational slide (sensu [1]) organized into several slide blocks (Figures 8 and 9). The movement (rotation) of blocks is greater towards the landslide toe, which may be interpreted as due to a retrogressive landslide. Initially, instability affects the lower parts of the slope, although as movement progressed, the upper parts of the slope became also unstable, increasing the size of the whole landslide. Upper blocks exhibited a lower displacement, and their effect on topography was reduced.

The results show that the thicknesses of both sandstone (reef sandstone and calcarenite) and red silt units are highly variable in the landslide area, with successive reductions and increases in thickness. As previously explained, this is interpreted as the effect of multiple failure surfaces cutting these geological units, causing the estimated changes in thickness. Because red silt units are also affected, it was deduced that the basal failure surface of the whole landslide should be found at the base of these units, and that intermediate failures root into this surface (Figures 8 and 9). This agrees with the contrast in shear strength of the involved materials, given the higher shear strength of basement materials compared with red silt unit (base of the Neogene sedimentary fill). The failure surface may hardly penetrate into the basement, and it more likely affects the sedimentary units or runs along the contact basin basement—red silt. In some cases, where the basement is deeper, basal failure occurs within the red silt unit (sections A–A′ and C–C′). This surface is found more than 60 m deep in the upper part of slide and about 50 m in its middle section.

The obtained results and the modeled cross-sections show the importance of two factors in the occurrence of this landslide. First, the valley suffered an intense process of erosion in the past, where river incision led to the erosion of most of the sedimentary fill (Figure 10). This undercut of valley slopes contributed to an initial destabilization of the slope. Additionally, a general dip of layers towards the free face of the slope also contributed to the general failure of the valley slope. From the proposed sections, the erosion has removed the sedimentary fill in section B–B′ (Figure 8), but there are still some remains of this fill in section A–A′ (and C–C′, Figures 8–10). It is reasonable to expect that river continues its incision (<1 mm/yr; [28]), but that it would be more effective on red silt (section A–A′) than in the marble and schist found in section B–B′ (Figure 8), so it is likely that the future evolution of this landslide would be more pronounced in its western flank. This is in agreement with displacement observed from interferometric techniques [30], which show that maximum displacements within the urban area of Albuñuelas occur just in the western part of the town (displacements above 2 mm/yr, with a maxima >12 mm/yr along the line of sight).

The framework of the landslide mechanism, which can be reconstructed following the geophysical investigations and the consequent refinement of the engineering–geological model of the slope on which the town of Albuñuelas stands, leads to the recognition of retrogressive dynamics of the landslide that, however, appears to concentrate its mobility in the portions of the slope that are already involved. The distribution of activities does not therefore appear to be widening. On the other hand, the progradation of the landslide mass seems to be disadvantaged by the intense erosion at its foot, caused by the Saleres River and evidenced by the deep incision of the deposits connected to the landslide mass itself. From a kinematic point of view, the landslide reveals the presence of numerous blocks, which are dislodged by secondary scarps and whose mobility can be distinguished with exposure to the possible reactivation of parts of the slope when trigger events, such as earthquakes, should occur.

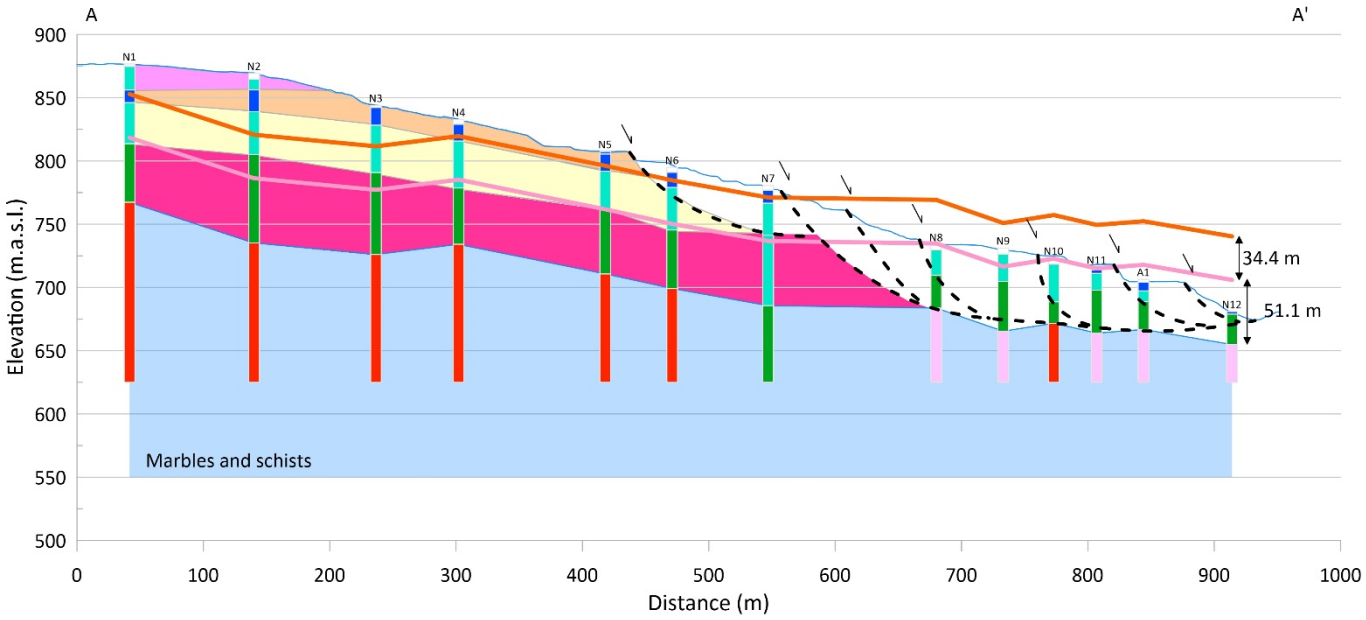

Figure 10. Estimated geometry of the valley slope before landslide occurrence for Section A–A′. Pink line: estimated position of top of red silt unites from average thickness of this unit in stable areas (Figure 7) and position of basement; orange line: estimated position of top of reef sandstone and calcarenite. Arrows mark the position of scarps in landslide body.

7. Conclusions

A combination of geological, geomorphological and geophysical techniques has been applied here to reconstruct the architecture and the failure mechanism of a large landslide affecting the town of Albuñuelas in southern Spain. Among these techniques, a particular role was played by seismic passive methods. An intensive and extensive usage of ambient noise allowed for the provision of a reliable seismic characterization of the area. The surveys of ambient noise measurements, carried out in this study, provided a general assessment of the fundamental resonance frequency and the thickness of the sedimentary layer, estimating the lateral extent of the landslide and the depth to the failure surface. The seismic passive methods are especially suitable thanks to their ability to identify physical properties of the subsoil, including its thickness and shear-wave velocity. The measure of these parameters can then be used to depict the size of the land mass. Advantages of these surface methods are mainly related to their non-invasive nature. They can be performed more rapidly than borehole methods and are less expensive than the one required for drilling. Furthermore, in sites that are difficult to examine, the surface methods may be the only choice for geotechnical investigations. Another important aspect of the surface methods is related to the volume of soil involved in the survey, wider than borehole methods. For all these reasons, the passive seismic measurements have been significantly growing in importance in the recent few years for the dynamic characterization of soil and landslide investigations. Furthermore, a strict synergy between geologic surveys, borehole and seismic surveys allow for the further reduction in relevant uncertainties during the data inversion.

The obtained results have allowed for the building of three cross-sections, showing the internal structure of this landslide. It is a rotational slide divided into several blocks with different degrees of displacement (rotation). The basal failure surface is found at more than 60 m in the upper parts of slide and about 50 m in its middle section, becoming shallower towards the toe. This study shows the importance of the river incision and erosion of the sedimentary fill of the basin, where an important part of it has been removed by river erosion, contributing to the destabilization of non-eroded parts of slope. Additionally, the results show that the general structure of the area, with materials dipping towards free face

of slope, also contributes to the landslide occurrence. Future evolution of this landslide will be controlled by the ability of the Saleres River to erode the bottom of the valley and by the materials found on it, which may lead to a different evolution of the western part, where soft materials exist in the bottom of the valley, with respect to the eastern part, where hard materials are found according to our results.

This research work constitutes the first step for future projects focused on understanding the behavior of this landslide due to different triggering factors (scenarios of intense rain periods, river undercut or severe seismic shaking).

Author Contributions: M.M.: Fieldwork, data integration and interpretation, and wrote the paper. J.J.G.-M.: Data interpretation and integration, and revised the manuscript. J.G.: Fieldwork, data integration and revised the manuscript. L.L.: Conceptualization of work, fieldwork and revised the manuscript. S.M.: Conceptualization of work, fieldwork, supervised interpretation and revised the manuscript. J.P.: Fieldwork, data interpretation and revised the manuscript. J.A.P.: Fieldwork, data integration and revised the manuscript. B.Y.N.B.: fieldwork. J.D.: Conceptualization of work, fieldwork, supervised interpretation and revised the manuscript. All authors have read and agreed to the published version of the manuscript.

Funding: This study was partially funded by the EU (FEDER), by the Secretaría de Estado de Investigación, Desarrollo e Innovación of the Spanish government (projects CGL2015-65602-R, CGL2016-77688-R), by the Spanish Investigation Agency (project PID2022-136678NB-I00 AEI/FEDER), by the Conselleria de Innovación, Universidades, Ciencia y Sociedad Digital de la Generalitat Valenciana (project CIAICO/2022/038), and by the Junta de Andalucía (project GGI3002IDIN).

Data Availability Statement: Raw data used in this study can be found here: http://hdl.handle.net/10045/138334.

Acknowledgments: The authors would like to thank the collaboration and support received from the research groups VIGROB-184 and VIGROB-116 (University of Alicante), the Institut Cartogràfic Valencia, the Agency Valencian Security and Response to Emergencies (Generalitat Valenciana) and the Provincial Consortium of Alicante Firefighters. We also acknowledge the collaboration of local authorities of Albuñuelas by providing all technical reports they had about landslides affecting this community.

Conflicts of Interest: The authors declare no conflict of interest.

References

1. Cruden, D.M.; Varnes, D.J. Landslide type and processes. In *Landslides. Investigation and Mitigation. Special Report 247*; Turner, A.K., Schuster, R.L., Eds.; Transportation Research Board; National Academy Press: Washington, DC, USA, 1996; pp. 36–75.
2. Duncan, J.M.; Wright, S.G. *Soil Strength and Slope Stability*; John Willey & Sons: Hoboken, NJ, USA, 2005; p. 312.
3. Jongmans, D.; Garambois, S. Geophysical investigation of landslides: A review. *Bull. Soc. Géol. Fr.* **2007**, *178*, 101–112. [CrossRef]
4. Rogers, J.D.; Chung, J. A review of conventional techniques for subsurface characterization of landslides. *Environ. Earth Sci.* **2017**, *76*, 120. [CrossRef]
5. Pazzi, V.; Morelli, S.; Fanti, R. A review of the advantages and limitations of geophysical investigations in landslide studies. *Int. J. Geophys.* **2019**, *2019*, 2983087. [CrossRef]
6. Méric, O.; Garambois, S.; Jongmans, D.; Wathelet, M.; Chatelain, J.L.; Vengeon, J.M. Application of geophysical methods for the investigation of the large gravitational mass movement of Séchilienne, France. *Can. Geotech. J.* **2005**, *42*, 1105–1115. [CrossRef]
7. Reyes-Carmona, C.; Galve, J.P.; Moreno-Sánchez, M.; Riquelme, A.; Ruano, P.; Millares, A.; Teixidó, T.; Sarro, R.; Pérez-Peña, J.V.; Barra, A.; et al. Rapid characterisation of the extremely large landslide threatening the Rules reservoir (S Spain). *Landslides* **2021**, *18*, 3781–3798. [CrossRef]
8. Perrone, A.; Iannuzzi, A.; Lapenna, V.; Lorenzo, P.; Piscitelli, S.; Rizzo, E.; Sdao, F. High-resolution electrical imaging of the Varco d'Izzo earthflow (southern Italy). *J. Appl. Geophys.* **2004**, *56*, 17–29. [CrossRef]
9. Szalai, S.; Szokoli, K.; Metwaly, M.; Gribovszki, Z.; Prácser, E. Prediction of the location of future rupture surfaces of a slowly moving loess landslide by electrical resistivity tomography. *Geophys. Prospect.* **2017**, *65*, 596–616. [CrossRef]
10. Méric, O.; Garambois, S.; Malet, J.; Cadet, H.; Guéguen, P.; Jongmans, D. Seismic noise-based methods for soft-rock landslide characterization. *Bull. Soc. Géol. Fr.* **2007**, *178*, 137–148. [CrossRef]
11. Imposa, S.; Grassi, S.; Fazio, F.; Rannisi, G.; Cino, P. Geophysical surveys to study a landslide body (NE Sicily). *Nat. Hazards* **2017**, *87*, S327–S343. [CrossRef]
12. Del Gaudio, V.; Wasowski, J.; Hu, W.; Capone, P.; Venisti, N.; Li, Y. Ambient noise and ERT data provide insights into the structure of co-seismic rock avalanche deposits in Sichuan (China). *Bull. Eng. Geol. Environ.* **2021**, *80*, 7153–7170. [CrossRef]

13. Delgado, J.; Galiana-Merino, J.J.; García-Tortosa, F.J.; Garrido, J.; Lenti, L.; Martino, S.; Peláez, J.A.; Rodríguez-Peces, M.J.; de Galdeano, C.; Soler-Llorens, J.L. Ambient noise measurements to constrain the geological structure of the Güevéjar landslide (S Spain). *Appl. Sci.* **2021**, *11*, 1454. [CrossRef]
14. Hussain, Y.; Schlögel, R.; Innocenti, A.; Hamza, O.; Iannucci, R.; Martino, S.; Havenith, H.-B. Review on the Geophysical and UAV-Based Methods Applied to Landslides. *Remote Sens.* **2022**, *14*, 4564. [CrossRef]
15. D'Amico, S.; Panzera, F.; Martino, S.; Iannucci, R.; Paciello, A.; Lombardo, G.; Galea, P.; Farrugia, D. Chapter 12—Ambient noise techniques to study near-surface in particular geological conditions: A brief review. In *Near-Surface Geophysics*; Persico, R., Piro, S., Linford, N., Eds.; Elsevier: Amsterdam, The Netherlands, 2019; pp. 419–460. [CrossRef]
16. Nakamura, Y. *A Method for Dynamic Characteristics Estimation of Subsurface Using Microtremor on the Ground Surface*; Quarterly Reports; Railway Technical Research Institute: Tokyo, Japan, 1989; Volume 30.
17. Aki, K. Space and time spectra of stationary stochastic waves, with special reference to microtremors. *Bull. Earthq. Res. Inst.* **1957**, *35*, 415–456.
18. Ohori, M.; Nobata, A.; Wakamatsu, K. A comparison of ESAC and FK methods of estimating phase velocity using arbitrarily shaped microtremor analysis. *Bull. Seism. Soc. Am.* **2002**, *92*, 2323–2332. [CrossRef]
19. Okada, H. *The Microtremor Survey Method, Geophysical Monograph Series 12*; Asten, M.W., Ed.; Society of Exploration Geophysicists: Tulsa, OK, USA, 2003.
20. Capon, J. High-resolution frequency–wavenumber spectral analysis. *Proc. IEEE* **1969**, *57*, 1408–1419. [CrossRef]
21. Lacoss, R.T.; Kelly, E.J.; Toksoz, M.N. Estimation of seismic noise structure using Array. *Geophysics* **1969**, *29*, 21–38. [CrossRef]
22. Bonnefoy-Claudet, S.; Köhler, A.; Cornou, C.; Wathelet, M.; Bard, P.Y. Effects of Love waves on microtremor H/V ratio. *Bull. Seismol. Soc. Am.* **2008**, *98*, 288–300. [CrossRef]
23. Parolai, S.; Mucciarelli, M.; Gallipoli, M.R.; Richwalski, S.M.; Strollo, A. Comparison of empirical and numerical site responses at the Tito Test Site, Southern Italy. *Bull. Seismol. Soc. Am.* **2007**, *97*, 1413–1431. [CrossRef]
24. Endrun, B.; Ohrnberger, M.; Savvaidis, A. On the repeatability and consistency of three-component ambient vibration array measurements. *Bull. Earthq. Eng.* **2010**, *8*, 535–570. [CrossRef]
25. Parolai, S.; Picozzi, M.; Richwalski, S.M.; Milkereit, C. Joint inversion of phase velocity dispersion and H/V ratio curves from seismic noise recordings using a genetic algorithm, considering higher modes. *Geophys. Res. Lett.* **2005**, *32*, L01303. [CrossRef]
26. Picozzi, M.; Parolai, S.; Richwalski, S.M. Joint inversion of H/V ratios and dispersion curves from seismic noise: Estimating the S-wave velocity of bedrock. *Geophys. Res. Lett.* **2005**, *32*, L11308. [CrossRef]
27. Chacón, J.; Irigaray, C.; El Hamdouni, R. Informe sobre exposición a riesgos derivados de los movimientos de ladera en Albuñuelas (Granada). Incidencia de las lluvias de noviembre a enero de 1996/97. Memoria Técnica. Ayuntamiento de Albuñuelas. 1997; 34p, + 3 Annexes.
28. IGN. *El Terremoto de Andalucía de 25 de Diciembre de 1884*; Instituto Geográfico Nacional: Madrid, Spain, 1980; 139p.
29. Chacón, J.; Irigaray, C.; El Hamdouni, R. Vuelco de viviendas de la población de Albuñuelas (Granada). Informe Final. Contrato Fundación Empresa-Universidad de Granada. Ayuntamiento de Albuñuelas. 2007; 43p, + 3 annexes.
30. Fernández, P.; Irigaray, C.; Jiménez, J.; El Hamdouni, R.; Crosetto, M.; Monserrat, O.; Chacón, J. First delmitation of areas affected by ground deformations in the Guadalfeo river valley and Granada metropolitan area (Spain) using the InSAR technique. *Eng. Geol.* **2009**, *105*, 84–101. [CrossRef]
31. Sanz de Galdeano, C.; García Tortosa, F.J.; Peláez, J.A.; Alfaro, P.; Azañón, J.M.; Galindo Zaldívar, J.; López Casado, C.; López Garrido, A.C.; Rodríguez Fernández, J.; Ruano, P. Main active faults in the Granada and Guadix-Baza Basins (Betic Cordillera). *J. Iber. Geol.* **2012**, *38*, 209–223. [CrossRef]
32. Stich, D.; Martínez-Solares, J.M.; Custódio, S.; Batlló, J.; Martín, R.; Teves-Costa, P.; Morales, J. Seismicity of the Iberian Peninsula. In *The Geology of Iberia: A Geodynamic Approach, Active Processes: Seismicity, Active Faulting and Relief*; Quesada, C., Oliveira, J.T., Eds.; Springer Nature: Cham, Switzerland, 2020; Volume 5.
33. Madarieta-Txurruka, A.; González-Castillo, L.; Peláez, J.A.; Catalán, M.; Henares, J.; Gil, A.J.; Lamas-Fernández, F.; Galindo-Zaldívar, J. The role of faults as barriers in confined seismic sequences: 2021 seismicity in the Granada Basin (Betic Cordillera). *Tectonics* **2022**, *41*, e2022TC007481. [CrossRef]
34. Braga, J.C.; Martin, J.M.; Alcala, B. Coral reefs in coarse-terrigenous sedimentary environments (Upper Tortonian, Granada Basin, southern Spain). *Sediment. Geol.* **1990**, *66*, 135–150. [CrossRef]
35. Fernández, J.; Viseras, C.; Soria, J. *Tertiary Basins of Spain. The Stratigraphic Record of 535 Crustal Kinematics*; Cambridge University Press: Cambridge, UK, 1996.
36. Avidad, J.; García-Dueñas, V.; Gallegos, J.A.; González Donoso, J.M. *Mapa Geológico de España, E:1:50.00, Hoja 1041 (Dúrcal)*; IGME: Madrid, Spain, 1981; 45p.
37. Martín-Suárez, E.; Freudenthal, M.; Agustí, J. Micromammals from the Middle Miocene of the Granada Basin (Spain). *Geobios* **1993**, *26*, 377–387. [CrossRef]
38. Reyes-Carmona, C.; Jabaloy, A.; Galve, J.P. Estructura del graben asimétrico de Albuñuelas (Granada). *Geogaceta* **2018**, *64*, 7–10.
39. Sanz de Galdeano, C.; López Garrido, A.C. Estructura y tectónica activa del valle de Lecrín. *Geogaceta* **2001**, *30*, 187–190.
40. D'Angiò, D. Caratterizzazione Meccanica di Laboratorio dei limi Argillosi della Successione del Rio de Albuñuelas (Granada, Spagna). Bachelor's Thesis, Facoltà di Scienze Matematiche, Fisiche e Naturali, Università di Roma–La Sapienza, Roma, Italy, 2013; 51p.

41. Román-Herrera, J.C.; Delgado, J.; Rodríguez-Peces, M.J.; Peláez, J.A.; Garrido, J. Evaluation of road network slopes susceptibility to seismically-induced landslides in the Granada Basin (S Spain). *Front. Earth Sci. Geohazards Georisks* **2023**, *11*, 1226894. [CrossRef]
42. Irigaray, C.; Lamas, F.; El Hamdouni, R.; Fernandez, T.; Chacon, J. The importance of precipitation and the susceptibility of slopes in the triggering of landslides along roads. *Nat. Hazards* **2000**, *21*, 65–81. [CrossRef]
43. El Hamdouni, R. Estudio de Movimientos de Ladera en la Cuenca del Río Ízbor Mediante un SIG: Contribución al Conocimiento de la Relación entre Tectónica Activa e Inestabilidad de Vertientes. Ph.D. Thesis, Universidad de Granada, Granada, Spain, 2001; 430p.
44. Lermo, J.; Chávez-García, F.J. Site effect evolution using spectral ratios with only one station. *Bull. Seismol. Soc. Am.* **1993**, *83*, 1574–1594. [CrossRef]
45. Lermo, J.; Chávez-García, F.J. Are microtremor useful in site response evolution. *Bull. Seismol. Soc. Am.* **1994**, *84*, 1350–1364.
46. Lachet, C.; Bard, P.-Y. Numerical and theoretical investigations on the possibilities and limitations of the Nakamura's technique. *J. Phys. Earth.* **1994**, *42*, 377–397. [CrossRef]
47. Field, E.H.; Jackob, K.H. A comparison and test of various site response estimation techniques, including three that are non reference—Site dependent. *Bull. Seismol. Soc. Am.* **1995**, *85*, 1127–1143.
48. Gitterman, Y.; Zaslavsky, Y.; Shapira, A.; Shtivelman, V. Empirical site response evaluations: Case studies in Israel. *Soil Dyn. Earthq. Eng.* **1996**, *15*, 447–463. [CrossRef]
49. Seekins, L.C.; Wennerberg, L.; Marghereti, L.; Liu, H.P. Site amplification at five locations in San Fransico, California: A comparison of S waves, codas, and microtremors. *Bull. Seismol. Soc. Am.* **1996**, *86*, 627–635. [CrossRef]
50. Fäh, D.; Rüttener, E.; Noack, T.; Kruspan, P. Microzonation of the city of Basel. *J. Seismol.* **1997**, *1*, 87–102. [CrossRef]
51. Albarello, D.; Lunedei, E. Alternative interpretations of horizontal to vertical spectral ratios of ambient vibrations: New insights from theoretical modeling. *Bull. Earthq. Eng.* **2010**, *8*, 519–534. [CrossRef]
52. Nogoshi, M.; Igarashi, T. On the propagation characteristics estimations of subsurface using microtremors on the ground surface. *J. Seism. Soc. Jpn.* **1971**, *23*, 264–280.
53. Gallipolli, M.R.; Albarello, D.; Mucciarelli, M.; Bianca, M. Ambient noise measurements to support emergency seismic microzonation: The Abruzzo 2009 earthquake experience. *Boll. Geofis. Teor. Appl.* **2011**, *52*, 539–559.
54. Foti, S.; Parolai, S.; Albarello, D.; Picozzi, M. Application of surface-wave methods for seismic site characterization. *Surv. Geophys.* **2011**, *32*, 777–825. [CrossRef]
55. Arai, H.; Tokimasu, K. S-wave velocity profiling by inversion of microtremor H/V spectrum. *Bull. Seismol. Soc. Am.* **2004**, *94*, 53–63. [CrossRef]
56. Sambridge, M. Geophysical inversion with a neighbourhood algorithm I. Searching a parameter space. *Geophys. J. Int.* **1999**, *138*, 479–494. [CrossRef]
57. Wathelet, M. An improved neighborhood algorithm: Parameter conditions and dynamic scaling. *Geophys. Res. Lett.* **2008**, *35*, L09301. [CrossRef]
58. Wathelet, M.; Jongmans, D.; Ohrnberger, M. Surface-wave inversion using a direct search algorithm and its application to ambient vibration measurements. *Near Surf. Geophys.* **2004**, *2*, 211–221. [CrossRef]
59. Acerra, C.; Aguacil, G.; Anastasiadis, A.; Atakan, K.; Azzara, R.; Bard, P.-Y.; Basili, R.; Bertrand, E.; Bettig, B.; Blarel, F. *Guidelines for the Implementation of the H/V Spectral Ratio Technique on Ambient Vibrations Measurements, Processing and Interpretation*; European Commission–EVG1-CT-2000-00026 SESAME; European Commission: Brussels, Belgium, 2004.
60. Galiana-Merino, J.J.; Mahajan, A.K.; Lindholm, C.; Rosa-Herranz, J.; Mundepi, A.K.; Rai, N. Seismic noise array measurements using broadband stations and vertical geophones: Preliminary outcomes for the suitability on f-k analysis. *Bull. Earthq. Eng.* **2011**, *9*, 1309–1325. [CrossRef]
61. Rosa-Cintas, S.; Galiana-Merino, J.J.; Rosa-Herranz, J.; Molina, S.; Giner-Caturla, J. Suitability of 10 Hz vertical geophones for seismic noise array measurements based on frequency-wavenumber and extended spatial autocorrelation analyses. *Geophys. Prospect.* **2012**, *61*, 183–198. [CrossRef]
62. Asten, M.W.; Henstridge, J.D. Array estimators and use of microseisms for reconnaissance of sedimentary basins. *Geophysics* **1984**, *49*, 1828–1837. [CrossRef]
63. Building Seismic Safety Council. *NEHRP Recommended Provisions for Seismic Regulations for New Buildings and Other Structures (FEMA P-750)*; Building Seismic Safety Council: Washington, DC, USA, 2009.